UAV-based Multiple Source Localization and Contour Mapping of Radiation Fields

Abdullah Al Redwan Newaz, Sungmoon Jeong, Hosun Lee, Hyejeong Ryu, Nak Young Chong

Abstract

This paper proposes an efficient approach to the multiple source localization and contour mapping problem of radiation fields using Unmanned Aerial Vehicles (UAVs). A typical radiation field originating from a single hotspot can be generated by three spatial distributions of sources; scattered, clustered and biased. Of these, the clustered sources are relatively easy to localize, because the sources are located in a close proximity to the center of distribution. In other cases, it is not very straightforward, because, when multiple radiating sources generate a hotspot in a cumulative manner, sources do not coincide with the hotspot position. Regardless of our knowledge about the hotspot position, we attempt to solve the multiple radiation localization problem in two steps: the Region Of Interest (ROI) selection and the source localization. Existing algorithms eventually explore whole area, causing the problem of excessive use of UAV resources. We therefore propose a framework to reduce ROI in a radiation field that not only optimizes the resources but also increases the localization accuracy. For the source localization process, two different methods are employed interchangeably. Those methods are called the Hough Transform and the Variational Bayesian, adaptively selected with a switching technique and the overall

*Abdullah Al Redwan Newaz

[1]The authors are with the School of Information Science, Japan Advanced Institute of Science and Technology, Ishikawa 923-1292. {*redwan, jeongsm, Hosun_LEE, hjryu, nakyoung*}*@jaist.ac.jp*

performance is evaluated by balancing between the localization accuracy and the required exploration. In favor of the optimization, the prediction model defines the type of sources in a way that the adaptive switching methodology can converge to an optimal solution by selecting an appropriate method. Thus, the proposed framework enables the UAV to accurately localize the radiation sources in a fast manner. In order to verify the validity and the performance of the proposed strategies, we performed extensive numerical experiments with different numbers of sources and their positions. Our empirical results clearly show that the proposed approach outperforms existing individual approaches.
Keywords: UAV, source localization, radiation mapping, topographic map

---

1. Introduction

After a nuclear accident, a radiation field can be generated by the leakage of radiation sources. As a disaster recovery plan, it is important to know the distribution of radiation levels over an area of interest, so that rescue mission could be accelerated to minimize the losses. In this kind of situation, autonomous flying robots such as Unmanned Air Vehicle (UAV) can be deployed to monitor the state of radiation effect, since using a UAV exploratory to autonomously gather the measurement of a radiation field keeps humans away from performing such a dangerous and life-risk task. Radiation sensors mounted on a UAV can detect the intensity in a radiation field, giving an indication of the activities of nearby sources. The inverse square relationship between the intensity of the radiation source and its distance from the observer can be used to lead the robot to the radiation sources by finding the maximum intensity value.

The search areas may span very large geometric distances, but the measurement attributes of a large radiation field is available only to the close proximity of the sources. Therefore, depending on the radiation leakages, several radioactively contaminated areas can be found in a large radiation field. Since nearby sources also cumulatively contribute to generate a hotspot, without losing the generality, we assume that only a single hotspot exists in each contaminated

area, which is caused by all the nearby sources. UAVs may be needed to fly over large a contamination area, which often leads to problems in designing the exploration strategy with limited resources *e.g.* limited battery life, sensing range and so on. All locations in a contaminated area are not uniformly important to explore for spatial localization of radioactive sources. Thus, an effective search strategy within a limited fraction of locations can facilitate efficient estimation of radiation source positions. Along this line, it is also important to estimate the distribution of radiation intensity on the geometric map, so that we can reduce our region of interest **(ROI)** not only for the field characterization but also for the source localization. Given reliable sensor model about the radiation field and accurate localization and navigation performance of the UAV, the goal of this paper is to plan an exploration strategy for the UAV to rapidly localize all the sources. A common solving method is to cover the whole target area so that a global picture of the radiation exposure of that area can be obtained. However, covering the whole area in this regard is not optimal since the UAV has to take account of the limited time constraints (partly due to the battery life).

Recent works estimate the sources in a radiation field using either Hough transformation (HT) [1] or Gaussian mixture [2]. When a radiation field comprises clustered sources, a standard way is to use the HT, especially when the sources are located at the center of the distribution. HT can significantly reduce the UAV exploration cost, allowing UAVs to determine the source positions by exploring only the contour line of the radiation intensity not far away from the sources [1]. However, the cumulative radiating effect of biased and scattered sources makes the field more complex to estimate,as the sources are not located in close proximity of the center of the distribution. Thus, the problem of estimating a radiation field, which is generated by the combination of multiple sources effect, is often considered as the problem to estimate components from a Gaussian mixture [2].

To balance the tradeoff between the exploration and the localization problems, an adaptive framework is proposed in this work, which can narrow down

the robotic exploration and concurrently accelerate the source localization processes. Thus, in this paper, given the hotspot location along with limited sampling of the radiation field, our aim is to answer the following question- how quickly and accurately can we localize all the radiating sources in a temporally invariant radiation environment?

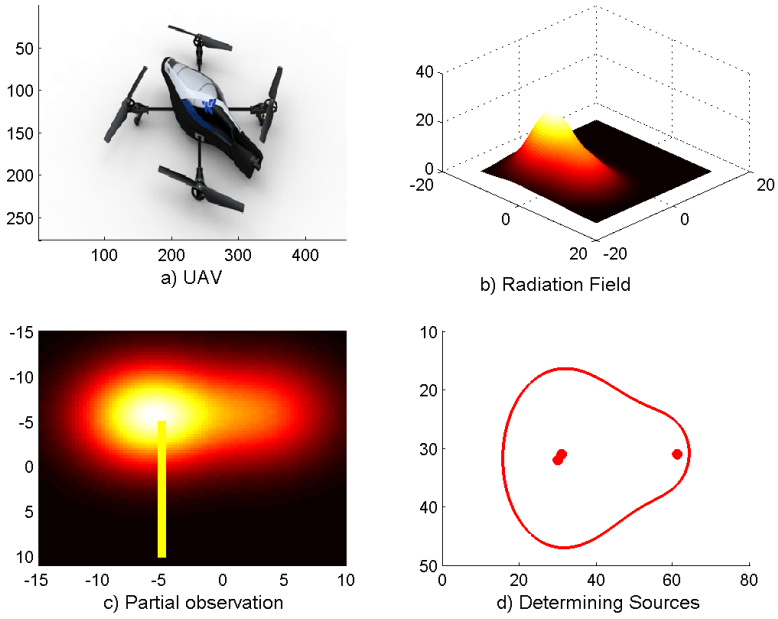

Figure 1: **Motivation:** UAV is deployed in a radiation field, shown in **(a, b)**. Given partial map (yellow line path and corresponding measurement), shown in **(c)**, it has to determine the ROI area (red line) and sources (red dots) using local sensing, shown in **(d)**. The measurement of radiation is indicated by colored map, shown in **(b, c)**.

To investigate this problem, we assume that an unknown radiation field might behave like either clustered sources or biased/scattered sources cumulatively generate a single hotspot. Starting off on the arbitrarily chosen initial position of the UAV, a hotspot directed trajectory is assumed to be given for our system (similar to Fig, 1 (c)). A conventional extremum seeking algorithm can easily generate this kind of trajectory [3, 4, 5]. However, we also assume

that each location in the trajectory is coupled with measurement attributes, which represents the joint strength of the sources (intensity). We contribute a classifier called log-gradient to determine the informative location form that trajectory. Under the assumption that the intensity of a contour line is constant value, the contour discovering processes generate a contour line for each informative location. We show that the reduction of region of interest can be possible by analyzing the similarity of contour shapes. Finally, focusing on the trade-off between the exploration cost and the localization accuracy, the proposed framework chooses an appropriate algorithm (namely HT or Variational Bayesian (VB)) to localize the sources.

Briefly speaking, the main contributions of this paper are as follow.

1) *Characterizing the cumulative radiation effects with multiple sources.*

2) *Finding the region of interest* ***(ROI)*** *in large radioactively contaminated areas to narrow down the search area.*

3) *Quickly and accurately localize the sources that are actively acting in the radiation field.*

To discuss the aforementioned topics, this paper is organized as follows: in Section 2, we investigate the work related in this area; in Section 3 we describe the field property characterization and rough classification based on partial data; Section 4, we present a complete geometric classification criteria based on the local sensing and our strategy to find ROI. Section 5, we briefly explain two different approaches to determine the sources and an adaptive switching methodology to balance the tradeoff between the exploration and the localization. Finally, in Section 6 and 7, we present experimental results and conclude our findings.

2. Related Work

The radiation field can be analyzed through a wide range of characterization techniques ranging from a point source to mixture models. Earlier works focus

on point source based field characterization [6, 7, 8], whereas more variations are found in recent literature. Recent researches have made significant progress in predicting spatial radiation field using Gaussian Process [9, 10]. However, when multiple sources are placed in an area showing cumulative effects, Gaussian Mixture Model **(GMM)** [2] is a well-suited method to characterize it. Of these choices, we use the GMM in our work to characterize a radiation field originating from multiple sources.

In order to illustrate the radiation effects over an area of interest, a radiation map is needed. A grid based map could have a finite number of rectangular cells [11] to represent the field property. On the other hand, we can explain the radiation field using topographic maps [12, 1]. In the topographic map, the field is characterized by large scale intensity measurements and quantitative representation of distribution using contour lines. Thus, it is very useful for the time-limited mission. To this end, our work present the first prediction model of the source locations by analyzing topographic maps.

Hotspot detection is often termed as a source seeking problem in the literature. Several strategies are applied to find a hotspot in an unknown radiation field. Those strategies are mostly divided into two categories, namely, model-free and model-based approaches. Specifically, model-free based approaches involve following a stochastic gradient of the radiation field intensity. It is observed that since the gradient of the intensity is followed, without a priori threshold limit (definition of the hotspot) those algorithms tend to converge to a neighborhood of a local maximum of the field [3]. In the context of model-based approach, source seeking can be performed using either the mutual information (MI) [3, 13] or MI gradient [4, 5]. While the popular approach for the source seeking task is to deploy a group of distributed robots [3, 14, 15], a single robot can travel to several locations in order to gather intensity measurements [16, 17, 18] as well as it is then possible to localize the hotspot with a predefined threshold value [3]. We exploit the source seeking algorithm to generate a UAV trajectory from an arbitrary intensity zone to the hotspot zone for prior knowledge of the field.

A numerous approach can be found in the literature to estimate the multiple

radiation sources. The Archimedian spiral search pattern [19] is basically an exhaustive search to determine the radiation sources within the target area. The Artificial Potential Field (APF) [20] based exploration in a radiation field might get confused more easily with the presence of multiple sources. Multi-robot adaptive sampling uses distributed robot exploration to classify radiation fields via recursive geometric subdivision [15]. If the map of the target area is a priori known, powerful algorithms like submodular optimization [21], mutual information gain [14], maximum entropy based path planning [22] can yield good results. Despite having a radiation map or an exhaustive search pattern, a key challenge in radiation field mapping is plagued with a limited flight time of the robot needed to find a ROI. This heckles the UAV in large-scale radiation field mapping.

In literature, we have seen that GMM based radiation field parameters can be estimated using a progressive correction technique [2], where a uniformly distributed sensor array was deployed in the area of interest. The sequence of distributions is successively approximated by the Bayes' rule. However, in our case the problem is complicated by the limitation of robotic exploration that gathers spatial measurement attributes of the field. To avoid the problem associated with limited exploration, we propose to use a topographic map to represent the large radiation field with a finite number of contour lines. Only a few efforts have been made to improve radioactive source detection using the topographic mapping strategy. Jerry Towler [7] used Archimedian spiral search patterns to gather measurements and discovered the contour lines with user-defined intensity values. He finally proposed to use the HT to estimate the source position. Although the performance of HT is satisfactory for the clustered sources, in contrast, it gives the worst results for the biased and the scattered sources respectively. Throughour empirical investigation, we demonstrate that our adaptive switching methodology not only optimizes the ROI but also persistently and accurately localizes the sources.

Fig. 2 shows all the necessary steps of our proposed algorithm. Although our source position estimation is also based on a topographic map, the pro-

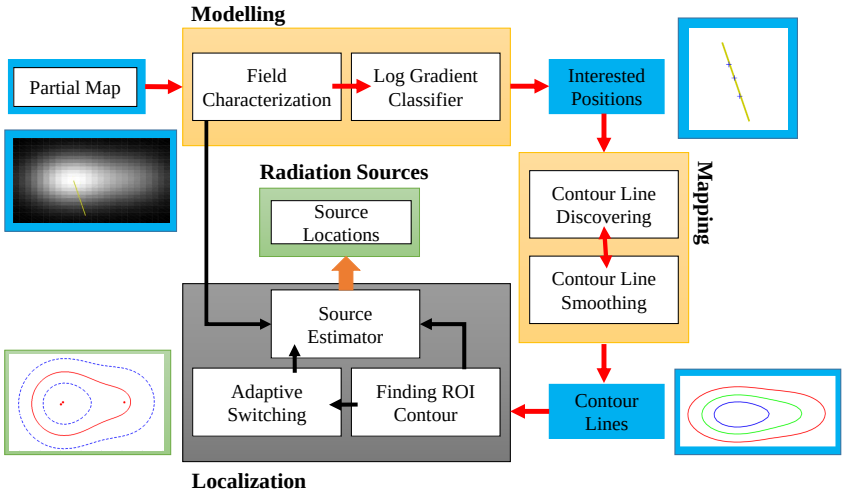

Figure 2: **System Overview:** A hotspot directed path coupled with measurement attributes is considered as a partial map for this system, it is denoted by the yellow line in the figure. The log-gradient classifier segmented to the partial map into a finite number of interested positions, denoted by (+) symbols. The topographic mapping processes generate the contour lines from the interested positions. The ROI contour is selected by the similarity analysis of the contoru lines. Two methods are studied to balance the tradeoff between the rapid localization and the precise localization. Thus, the adaptive switching methodology selects the best method to pursue the rapid and precise localization objectives. The blue boxes are the output of each process. The yellow boxes, including red arrows, are the processes for ROI selection. The gray box and black arrows are the process of source localization.

posed approach differs significantly than [7]. First, from a given partial map, we find a set of interested measurement attributes (intensity values) coupled with the position information using our novel log gradient classifier. Started with the initial positions, multiple contour lines are generated by tracking identical intensity values. Secondly, the ROI contour line is automatically chosen using contour shape analysis. Finally, instead of a single method -which cannot optimize all type of distributed sources, we propose a self-adaptive framework to select the appropriate method to localize the source positions in the most efficient manner.

3. Radiation Field Modelling

There are significant differences between geographic mapping and radiation distribution mapping [11]. In this work, we aim to include the radiation intensity and its distribution on top of a geographic map, based on the assumption that the UAV localization error is negligible. In our radiation mapping problem, we assume that a partial observation of the field is given, but the overall radiation distribution is unknown. Partial observation can be found, for instance, observing a UAV trajectory coupled with measurement attributes of the radiation field. It is necessary that the UAV trajectory connects an arbitrary intensity zone to the hotspot so that a rough estimation of the radiation field can be made initially. While the accurate radiation map can be obtained at the expense of exhaustively exploring the area, it is desirable to develop an efficient and effective mapping method considering the limited resources of UAVs. In this paper, we categorize the field, so that the UAV does not need to visit all the terrains, but rather to explore only the ROI contour or the area bounded by the ROI contour to localize the sources.

In this section, we explain the procedure to characterize the radiation field using **GMM**. Next we explain how to incorporate prior knowledge. Using the log-gradient classifier, we segment the partial map into several interested positions.

3.1. Field Characterization

The intensity in the field could change gradually or abruptly depending on the source location. A region could have high intensity values because of the influence of multiple sources or the presence of strong nearby sources. Hence, it is not plausible to detect individual sources because of unknown diffusion information about each source. In order to predict their possible location, we attempt to show their effect in the geographic map, adding the distribution of radioactive intensity on the map. In other words, the cumulative radiation effect of the sources is unlikely to be represented using a unimodal Gaussian model. For this reason we use **GMM** to characterize the radiation field. Let $x \in \mathbf{X}$ represents the location of the field and $z(x) \in \mathbf{Z}$ represents the corresponding measurement. The field property is characterized using GMM with M components such that

$$F_m(x; \alpha, \mu, \Sigma) := \sum_{b=1}^{M} \frac{\alpha_b \phi(x - \mu_b)}{{\Sigma_b}^2} \tag{1}$$

where $\phi(x) = \exp\left(-\frac{||x||^2}{2}\right)/(2\pi)$; $\mu_1, ..., \mu_M$ are the means; $\Sigma_1, ..., \Sigma_M$ are the variances and $\alpha_1, ..., \alpha_M$ are the mixing weights that describe the Gaussian components. The mixing weights are non-negative and added up to one. In order to generate the ground truth, we assume that each component has equal strength and the relative distance between each mean and measured location has influenced α. However, in our case α is equally divided by the number of sources (M), and the variance (Σ) is not important to localize sources. Therefore, we only need to estimate the mean (μ) of the sources using VB.

3.2. Log-gradient classifier (lgc)

The log-gradient classifier works like a rounding function for grouping the partial map. It converts the partial map into a finite number of interested positions based on the numerical relationship. Let $x_{i=0}$ is the robot initial position, $x_{i=h}$ is the hotspot location and i is the element index of the partial map, $i : \mathbb{R}^3 \to \mathbb{N}$. Also let the function $z(x_0, x_i)$ is the measurement attribute

of the corresponding location x_i w.r.t. x_0 such that $z : \mathbb{R}^2 \rightarrow \mathbb{R}$. Let, draw a line as shown in Fig. 1(c) connecting the robot position. The line also contains the measurement attributes based on the region of the colored radiation map. Therefore, the partial map is the set of a small section of the field including the corresponding measurement attribute. Our target is to group the partial map in an efficient way. First, we investigate how the measurement varies w.r.t. the robot position by taking gradient at a map index i given by

$$\nabla_i = \frac{z\left(x_0, x_i\right)}{d\left(x_0, x_i\right)} \tag{2}$$

where, $d(x_0, x_i)$ is the distance functions w.r.t. the initial position of the robot. However, in order to group the different zones into the same layer, we rather focus on the power of gradient values given by

$$\log\left(\nabla_i\right) = \log\left(\frac{z\left(x_0, x_i\right)}{d\left(x_0, x_i\right)}\right) \tag{3}$$

The log-gradient operator classifies the partial map using Eqn. (3), which is dependent on the precision value, Λ, to get the number of classified regions $x_{\hat{\mathbf{j}}}$, where $\hat{\mathbf{j}} \in \mathbb{N}^m$ is the index set that contains a subset index of the partial map locations. In short, the input of the log-gradient classifier (lgc) are a partial map which is a set of explored locations coupled with measurement attributes, $< x_{0:h}, z_{0:h} > \in \mathbb{R}^{n\times 3}$, and a user defined precision value Λ, resulting in the output set which is the classified regions coupled with the measurement attribute $< x_{\hat{\mathbf{j}}}, z_{\hat{\mathbf{j}}} > \in \mathbb{R}^{m\times 3}$. Note that the dimension of the classified regions m is smaller than the dimension of the partial map n. The operation of lgc can be expressed as follows

$$\mathrm{lgc}\left(< x_{0:h}, z_{0:h} >, \Lambda\right) :=< x_{\hat{\mathbf{j}}}, z_{\hat{\mathbf{j}}} > \tag{4}$$

The sequence of interested positions starts from the hotspot location and terminates at the outward periphery such that $\hat{\mathbf{j}} = \{h : m\}$ in Eqn. 4. Intuitively, we can say that if Λ is a high value (say 8 digits after the decimal point), the classified regions are more in terms of dimensions, results in more number of interested positions shown in Fig. 2.

4. Topographic Mapping

Based on the initially assigned positions by the *lgc*, the whole contour line is discovered in the contour generation phase. We use the intensity information to track a contour line. It is known that intensity along the contour line is a constant value, the robot then discovers the contour line by mapping the measurement gradient into the geometric domain. However, it is beyond the scope of this paper to summarize the state of the art in detector model; our overall approach is concerned about the robotic exploration and is not restricted to a specific sensor model. Without loss of generality, we will restrict our discussion to the exploration strategy along with measurement uncertainties. Note that as defined by the *lgc*, we start contour discovering algorithm relative to the nearest distance from the hotspot so to adaptively stop contour generation phase.

4.1. Contour line discovering

Let us denote the robot position at time t as $\mathbf{x}_t = \{x_t, y_t\}$, where a well known Cartesian coordinate. However, it is well known that drawing a contour line is relatively easier in Polar coordinate system, that motivates us to compute the robot position in Polar coordinate. The conversion from the Cartesian coordinate to the Polar coordinate system is simple and given by

$$\begin{aligned} r_t &= \sqrt{(x_t - x_0)^2 + (y_t - y_0)^2}, \\ \theta_t &= \arctan\left(\frac{y_t - y_0}{x_t - x_0}\right), \end{aligned} \tag{5}$$

where x_0 and y_0 are the initial positions. In order to draw a contour line, we transfer the reference point of the Polar coordinate to the hotspot location x_h. let, r is the radial distance from the reference point to the robot location. When the robot executes a control action, its next best location is given by a process model $\mathbf{x}_{t+1} = g(\mathbf{x}_t, r_t, \theta_t)$, where θ is the polar angle which range is 0 to 2π. By recursively update the polar angle and the radial distance, a contour line over the robot positions can be discovered.

Fig. 3 (a) shows the geometric analysis of a contour line. Let, at each iteration step, we adjust the radial distance and the polar angle as follows

$$\begin{aligned} r_t &= r_{t-1} + \delta r, \\ \theta_t &= \theta_{t-1} + \delta\theta, \end{aligned} \tag{6}$$

where δr is the radial increment of r, where $\delta r \in \mathbb{R}_+$ and $\delta\theta$ is the angular increment of θ, where $\delta\theta \in \mathbb{R}_+$. Note that, if δr is 0 and $\delta\theta$ is $Constant$, the robot will discover a circular contour line. However, the goal of the contour discovering algorithm is to infer the robot position at each step based on knowledge of the observation of field strength (defined as intensity I).

Let c_r is the contour length in geometric domain while c_I is the contour length in intensity domain. The goal is to estimate the contour line in geometric domain by tracking the contour line in intensity domain. After each motion, the robot receives measurement attribute z_t of the field according to its current position x_t. The observation of the contour line in an intensity domain is given by a measurement model $I = h(z_t, z_\mu, z_w)$, where z_μ is the target intensity sets for the intensity tracking and z_w is some unknown white noise added to model the measurement uncertainty. Starting off an arbitrary position on the contour line assigned by the lgc, the contour discovering algorithm repeatedly use the measurement gradient information to map the geometric contour line by estimating an unknown scale λ such that

$$c_r = \lambda \cdot c_I, \tag{7}$$

where the length of c_r is given by

$$c_r = \int_0^{2\pi} r^2 + \left(\frac{\delta r}{\delta\theta}\right)^2 \delta\theta, \tag{8}$$

and the length of c_I is given by

$$c_I = \int_0^{2\pi} I^2 + \left(\frac{\delta I}{\delta\theta}\right)^2 \delta\theta. \tag{9}$$

Since the lgc initially assigned the values of r and I in Eqn. 8 and Eqn. 9, the main challenge is to compute the scale λ that maps the δI and δr. Next, we will

show how to incorporate the measurement gradient information to accurately estimate the contour line in geometric domain.

4.2. Accurate Estimation

As it is obvious from Eqn. 6 that at each iteration step the robot has to infer the radial distance of the next location, the measurement uncertainties as well as the prediction uncertainties may lead the robot along the inaccurate contour line. Therefore, in this subsection, we introduce a recursive Bayesian filter to cope with the above mentioned uncertainties.

The contour line over the geometric domain can be discovered by discretizing the polar angle θ_t into a constant increment $\delta\theta \in \mathbb{R}_+$. Given the current polar angle θ_t, the robot estimates the radial increment $\delta r_t|\theta_t$ at each iteration step. After that, it computes the intensity gradient $\delta I_t|\theta_t \in \mathbb{R}$ as follows

$$\delta I_t|\theta_t = z_t - z_\mu + z_w \tag{10}$$

where z_μ is the target intensity, z_t is the current measurement attribute and z_w is Gaussian white noise. Note that the intensity gradient could be a positive or a negative value depending on the sensing locations. In order to apply this gradient information in geometric domain, we use a recursive Bayesian filter to compute the optimal scale λ given by

$$\lambda = \delta r_t|\theta_t \cdot \delta I_t|\theta_t \cdot \left(\delta r_{(t-1)}|\theta_t\right)^{-1} \tag{11}$$

Since the recursive Bayesian filter summarizes the current estimation $\delta r_t|\theta_t \cdot \delta I_t|\theta_t$ with the respect to the immediate past $\delta r_{(t-1)}|\theta_t$, as more observations are made, the scale will begin to converge to the true value. However, given a polar angle θ_t, when the estimated scale λ is a large value, the robot has to travel a long radial distance r, which can cause a huge prediction uncertainties. If we do not minimize that uncertainties, it will be propagated throughout the Bayesian filter into the future estimation, results in poor estimation accuracy.

Here we propose to optimize the polar angle increments to compensate for the discrepancy between the desired polar angle θ_t and the radial distance r as

follows

$$\delta\theta_t|r_t = atan\left(\frac{\delta\theta_t^2}{r_t^2}\right) \tag{12}$$

In this case a large radial increment is discretized by reducing the polar angle given by

$$\theta_t = \theta_t - \delta\theta_t|r_t \tag{13}$$

Algorithm 1 summarizes the overall estimation method. Note that each iteration step the predicted polar angle increment is a constant value, but the effective polar angle update is consistent with the optimal scale. Fig. 3 (b) represents the exploration strategy to discover an unknown contour line in the geometric domain.

Algorithm 1 Contour discovering

Require: initial r, initial θ, initial δr, constant $\delta\theta$

Ensure: Contour line in geometric domain

1: **Predict radial distance**

$r_{(t|t-1)} = r_{(t-1|t-1)} + \delta r_t|\theta_t$

2: **Predict polar angle**

$\theta_t = \theta_{t-1} + \delta\theta$

3: **Compute measurement residual**

$\delta I_t|\theta_t = z_t - z_\mu + z_w$

4: **Compute optimal scale**

$\lambda = \delta r_t|\theta_t \cdot \delta I_t|\theta_t \cdot \left(\delta r_{(t-1)}|\theta_t\right)^{-1}$

5: **Update radial increment**

$\delta r_t = \lambda \cdot \delta r_t$

6: **Update radial distance**

$r_t = r_t + \delta r_t$

7: **Update polar angle increment**

$\delta\theta_t|r_t = atan(\delta\theta_t^2/r_t^2)$

8: **Update polar angle**

$\theta_t = \theta_t - \delta\theta_t|r_t$

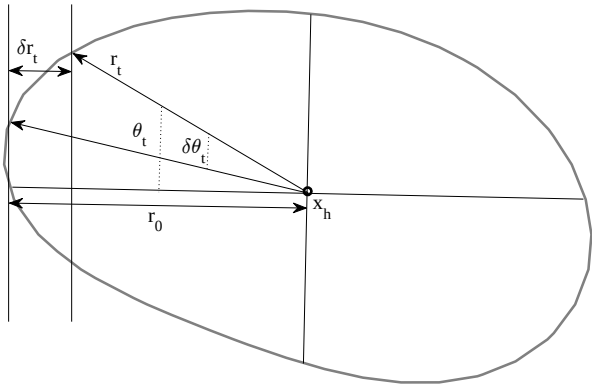

(a) Analysis of a contour line geometry.

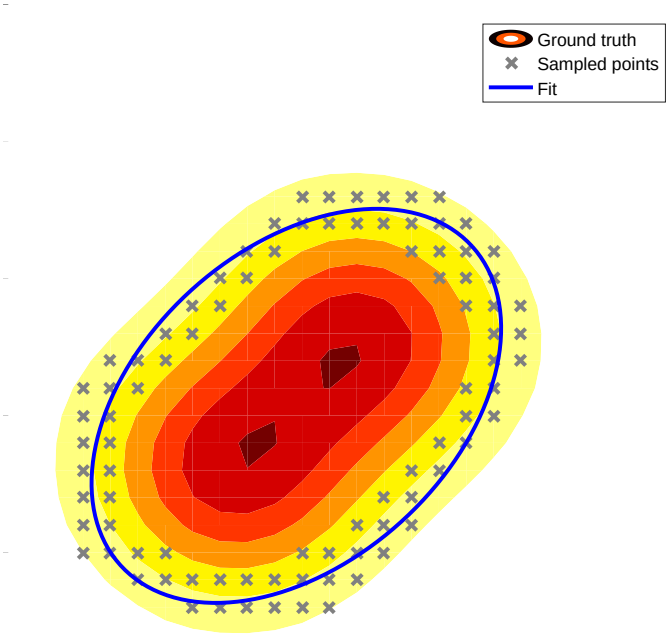

(b) Contour line exploration

Figure 3: Contour discover: A contour is discovered by recursively updating the radial distance and the polar angle using a Bayesian filter.

4.3. Finding the ROI contour

A topographic map may contain multiple contour lines depending on precision value (Λ) of the designed. However, all the contour lines are not important to explain the characteristic property of distribution. Obviously, contours near to the hotspot region are very important, since they help us visualize anisotropic, dynamic changes in the intensity of the radiation field. As the contour line goes outwards from the hotspot, the shape tends to be quite similar to each other. Therefore, we can analyze the contours shapes whereby the robot can terminate the exploration.

The previous contour line discovering process was designed to discover all the contour lines. Based on that process, we can find $\hat{\mathbf{c}} = \{c1, c2, .., cl\}$, which is the set of contour lines. Note that c_r, c_I are the length of each contour line in the geometric domain and the intensity domain respectively, whereas $\hat{\mathbf{c}} \in \mathbb{R}^l$ is the index set of all contours and l is the dimension of that set. We consider the global Cartesian coordinate system in order to analyze the degree of similarity between neighboring contour lines. For this we introduce the elements σ_x and σ_y, at each exploration in the contour discovering process to compute the relative changes of initially assigned radius, r_0, to the radius, r_t, at current exploration step given by

$$\begin{aligned} \sigma_x &= \{(r_t - r_0)\cos(\delta\theta)\}, \\ \sigma_y &= \{(r_t - r_0)\sin(\delta\theta)\}. \end{aligned} \tag{14}$$

It is obvious from the above equation that $\hat{\boldsymbol{\sigma_x}} = \left\{ \bigcup_t {\sigma_x}^t \right\}$ and $\hat{\boldsymbol{\sigma_y}} = \left\{ \bigcup_t {\sigma_y}^t \right\}$ represent the change in the radius w.r.t. the global Cartesian x-axis and y-axis respectively. Next, we will analyze the similarity between two neighboring contour lines by defining a function given by $\Gamma : \mathbb{R}^{l\times 2} \rightarrow \mathbb{R}$. We compute a score for each contour line w.r.t. the neighboring contour line closer to the hotspot using the following equation such that

$$\Gamma^* = \tan^{-1} \frac{E\{\hat{\boldsymbol{\sigma_x}}\}^2}{E\{\hat{\boldsymbol{\sigma_y}}\}^2} - \Gamma, \tag{15}$$

where Γ^* is the current contour score and Γ is the neighboring contour score. when Γ^* reaches a predefined tolerance limit, adding a new contour would be

redundant. Therefore, the robot can stop its exploration and narrow down the **ROI** to the previous contour such that

$$ROIC = \arg\min_{l} \left\{ \max_{\Gamma^* \in \Gamma^l} \left\{ \Gamma^l \left(cl, c(l-1) \right) \right\} \right\}. \tag{16}$$

where, $ROIC$ is the region of interested contour index.

5. Radiation Sources Localization

In this section, we briefly explain two different approaches to the localization of the radiation sources, namely HT and VB inference. The HT approach is reasonably accurate if we deal with the clustered sources only. It can localize the source position by exploring only to the ROI contour line. When the source distribution is somewhat uniformly scattered or biased, a potentially more accurate estimation than the HT can be obtained by the VB inference. The particular VB approach used here is based on the importance sampling which involves drawing samples from the ROI. In the context of ROI, a dense sampling can be performed within the bounded region, so that the estimation of the VB can converge to the true sources positions. Note that the main VB algorithm takes account of measurement uncertainties while estimating the source positions. Therefore, we will skip the additional explanation of the measurement uncertainties for the VB algorithm. On the other hand, the measurement uncertainties of the HT algorithm caused by the fact of the contour line discovering, which is already discussed in earlier section.

5.1. HT based source localization

The Hough Transform (HT) is a very useful tool to solve the computer vision and the image processing problems. Although HT is typically used to detect lines, it has been applied to the radiation sources detection problem in [1]. Since only contour lines are required to localize sources, it should be straightforward to use the conventional HT in the rapid source localization mission. In order to implement HT to localize the sources, first, the detected contour lines are

converted to a binary image. Secondly, the binary image is downsampled to one half to one quarter the original resolution to reduce the computational burden. Thirdly, the Hough circles are chosen by deterministically defining the maximum and minimum length of the radius parameters. Finally, the transform process can determine the center of each circular distribution.

However, for the HT has several major disadvantages, especially when applied to unknown radiation distributions. First, the determination process of the Hough circles is sensitive to the radius parameter. Without a good radius parameter, HT cannot accurately estimate the source positions. Furthermore, it is observed that HT can perform well when sources are clustered within a comparatively small area and their effects are approximated by a Gaussian distribution. It can therefore be concluded that, the applications of the HT in the source localization process is likely to be limited and source distribution type-specific.

A significant advantage of the HT over the VB is that it does not require information regarding the whereabouts of ROIs. We therefore use the HT to optimize exploration for the clustered sources, where the ROI contour localizes the sources with reasonable accuracy. The pseudo-code for the HT algorithm is given in Algorithm 2. In our simulation the convenient radial upper bound is the size of the image, while the lower bound is one ninth of the image size. The matlab function we use here is *houghcircles* that detects the center of the radiation sources.

5.2. VB inference based source localization

The exploration goal of the robot in this subsection is to gather the measurement attribute for a set of sensing locations which is bounded by the ROI contour line. Estimating radiation sources with given a set of measurements is commonly reffered to as inverse problem. The inverse problem is difficult by the fact that different regios could have the same intensity value. However, in our proposed framework, the ROI contour line can provide an additional information of the measurement distribution in geometric domain. Therefore, we

Algorithm 2 Hough Transform

Require: ROI contour

Ensure: Sources

1: **Convert the contour to a binary image**

$cImage = cnt2bin(contour)$

2: **Determine the parameters**

$maxRadius = size(cImage)$

$minRadius = maxRadius/9$

3: **Localize the sources**

$centers = houghcircles(cImage, maxRadius, minRadius)$

here contribute a probabilistic kernel function, so that the distribution of sensing locations along with their corresponding measurement attributes can jointly compute the maximum likelihood for the VB algorithm, results in improved estimation accuracy.

Let $\mathcal{P}$ is the exploration path that traverses each of the sening location at most one time. With slightly abusing the notation, assume that a location of the path $x_s \in \mathcal{P}$ pairs with the measurement attribute of that location z_s generates a sample point $< x_s, z_s >$. After traveling the path $\mathcal{P}$, the robot finds all the sample points bounded by the ROI contour line, which is then used to compute a probabilistic kernel function given by

$$k(\forall z_s) = \frac{1}{2 + \exp(\forall z_s)}. \tag{17}$$

Although we have gathered the measurement attribute, the actual sources are hidden variables. In order to estimate the source positions, firstly, we characterize the ROI area as an unknown GMM. Secondly, based on the measurement attribute, the parameters of the GMM are obtained by computing a maximum likelihood. The goal of the kernel function is to bias the distribution of sensing location to compute the maximum likelihood of the VB as follows

$$p(\forall x_s | \forall z_s) = \mathcal{N}(\forall x_s, \mu\,(x_s)) - k(\forall z_s), \tag{18}$$

where $\forall x_s$ is a column vector contains all the sensing locations information and $\forall z_s$ is also the column vector of corresponding measurements, thus, the normal distribution $\mathcal{N}(\forall x_s, \mu\,(x_s))$, the probabilistic kernel $k(\forall z_s)$ are also a column vectors respectively. Finally, the optimal number of components for Bayesian GMM can be obtained iteratively using a variational EM algorithm [23], which is achieved through partially performing an E-step and observing the maximization of E-step and M-step using the same function $F[q, \pi]$ such that

$$F\,[q, \pi] = \sum_{x \in \forall x} \int q\,(\forall z, \mu, \mathrm{T}) \log \frac{p\,(\forall x, \forall z, \mu, T; \pi)}{q\,(\forall z, \mu, \mathrm{T})} \partial\mu \partial T, \tag{19}$$

where the parameters (μ, T, π) are the mean (center) of the sources, the precision matrices and the mixture weights respectively. q is the arbitrary distribution that approximates the posterior distribution defined by

$$p\,(\forall x, \forall z, \mu, T; \pi) \overset{def}{=} p\,(\forall x | \forall z, \mu, T | \forall x; \pi)\,. \tag{20}$$

From Eqn. (18), we can see that uniform sample points inside the **ROI** area are explicitly biased towards the significant measurement attribute, which results in conversion of cluster samples. Therefore, the VB can easily estimate the optimal number of sources and their corresponding locations. The detailed formulas for computing the parameters can be found in [23]. In summary, at each iteration, the VB performs two following steps:

- **Variational E-Step:** Evaluate $q^* = \arg\max_q F\,[q, \pi]$
- **Variational M-Step:** Find $\pi^* = \arg\max_\pi F\,[q^*, \pi]$

A notable property of this model is that when maximizing F, the prior distribution of μ and T penalize the overlapping components, therefore the redundant sources whose effect are negligible to the distribution, are eliminated. Furthermore, it is sufficient to find the mean μ components to estimate the source position. We use an open source MATLAB function [24] to implement VB.

Algorithm 3 Variational Bayesian

Require: ROI contour, exploration path $\mathcal{P}$

Ensure: The number of sources and their corresponding positions

1: Generate the sample points by traveling $\mathcal{P}$.

2: Compute the probabilistic kernel function using the Eqn. (17).

3: Compute the maximum likelihood function using the Eqn. (18).

4: Estimate the number of sources and their corresponding positions using the Eqn. (19).

5.3. Adaptive switching strategy

The HT and VB methods described in earlier sections are now selectively used. We propose an switching method supported by the ROI selection scheme presented in the previous section, allowing the method to rapidly converge to a solution despite the lack of prior knowledge of the radiation field.

Similar to the ROI selection process, the variance slope of each contour lines can be used to estimate the distribution of source positions. Note that the sources are different than the measurement distribution. According to our findings, the variance slope as described in the previous section exhibits the following three characteristic properties such that

1) **Increasing order of the slope gradient :** In this category, the variance slope decreases from the outer periphery to the hotspot periphery. We observed that biased sources exhibit this type of behavior, because the inner contour line of biased sources is almost circular and outer contour lines are elongated along a specific direction. Thus, the variance slope converges from an elliptical and irregular circular shape to a (nearly) round shape.

2) **Decreasing order of the slope gradient :** Unlike the previous definition, the contour shape of a scattered sources is propagated from the nearly round to elliptical and irregular circular shapes while approaching

to the inner contour. Therefore, the variance slope exhibits a decreasing property while stepping towards inner contour lines.

3) **Constant order of the slope gradient :** When sources are positioned close to each other, all the contour lines detected by the exploration, basically turns out to be uniform circular shapes. Thus, the variance slope remains at a nearly constant level. We found that this is the case for the clustered sources.

An optimized active exploration performance, as described in the earlier section, can be achieved by selecting an to appropriate method. In detail, the HT can be applied only for the constant order of the gradient slope property. On the other hand, the VB can be used to tackle the increasing and decreasing order of the gradient slope properties. Choosing an appropriate method by this strategy alleviates the need for superfluous exploration. It is observed that without the proposed selection method can localize the sources with improved accuracy. However, the challenging part is fast and accurate analysis of the ROI contour.

6. Simulation Result

We have performed an extensive simulation validation of our algorithm in the different settings of the sources. Our first experiment focuses on reducing ROI in the radiation field depending on measurement distribution. Next, we extend the experimental settings to evaluate the source localization strategy. Finally, we analyze the effect of the ROI selection to the source localization, and also show that the proposed adaptive method optimizes the tradeoff between exploration and localization accuracy. However, the partial map given to this system does not depend on specific initial positions. It just contains the rough idea of the intensity distribution from lower to higher zones. In summary, we have shown that the ROI selection is very important since it can reduce the traversed path and enhance the estimation accuracy. Furthermore, we have also shown that under what condition we can extremely reduce the traversed path.

6.1. Reducing ROI

The partial map of the environment contains the UAV trajectory and corresponding measurement up to the hotspot location. The *log-gradient classifier (lgc)* classifies the trajectory depending on the measurement change. The main advantage of *lgc* is that it automatically segments the trajectory depending on the numerical properties of the measurement, resulting in a finite number of groups. Each group contains the starting position and the corresponding measurement value. It is then further explored to determine the whole line through the contour discovering process. We perform three experiments in determining ROI contour where sources are distributed in such form as scattered, clustered and biased respectively.

Fig. 4 represents our experimental situations, where the contour lines are drawn by mapping the intensity changes into the geographic domain. The background gray colored map is the distribution of the measurement, while the yellow line represents the given trajectory of UAV, which is also the partial map that fed to *lgc*.

Although *lgc* segmented the field into a finite number of groups, the similarity analysis of contour shape allows us to reduce the contour numbers further more. The similarity slope varies depending on the distribution. As can be seen in Fig. 4 (c), (g), (k), the similarity slope between two consecutive contours reach to a saturation level after a certain period. When the slope gets saturated, we can discard the current contour and fix our ROI onto the previous one, which explains why the ROI contours in Fig. 4 (d), (h), (l), are $2, 1, 2$ respectively.

6.2. Source Estimation

In this scenario, we have extended our experiments to source localization. After determining the ROI contour, we consider how the sources are localized. Fig. 5 shows the overall procedure of the algorithm, where the partial map in Fig. 4 (i) is discretized using the *lgc* and a finite number of contours are drawn using the topographic mapping process. Among the traversed contours, the ROI contour is selected for further exploration. Samples are taken uniformly from

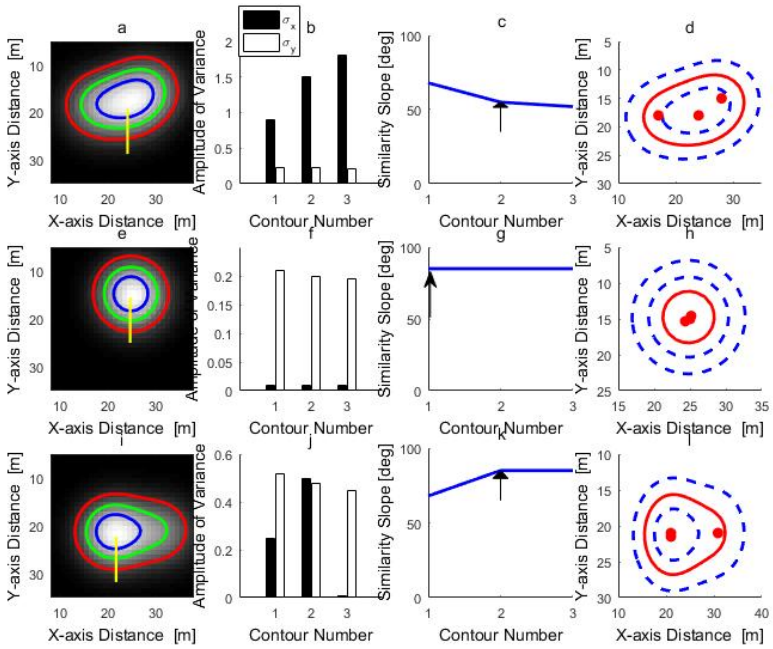

Figure 4: **Finding ROI contour:** The evaluation of the ROI contour computed by similarity analysis. Three different experiments are conducted namely scattered sources (a-d), clustered sources (e-h) and biased sources (i-l). The blue, green, red contours in (a,e,i) are labeled as (1,2,3) in (b, c, f, g, j, k). The variance of each contour computed over circular path while the similarity slope between two consecutive contours computed using Eqn. (16). The arrow in (c, g, k) indicates the starting position of similar contours. Finally the red contour line shown in (d, h, l) represents the ROI contour where the red dots are the actual sources.

the area bounded by the contour. The red circles in Fig. 5 (b), (e), (h), are the uniform sample locations. It can be seen from Fig. 5 (a), (d), (g), the sampling region is bounded by an approximate region of $30m \times 25m$, while our initial area of interest was at most $15m \times 15m$. The result suggests that a significant reduction is made in the ROI. This improvement is achieved by the similarity analysis of contour lines.

Since the number of estimated sources are not equal to the actual sources, the performance of algorithm is measured by computing the distance to the nearest estimated source. Table 1 shows the difference between the VB and

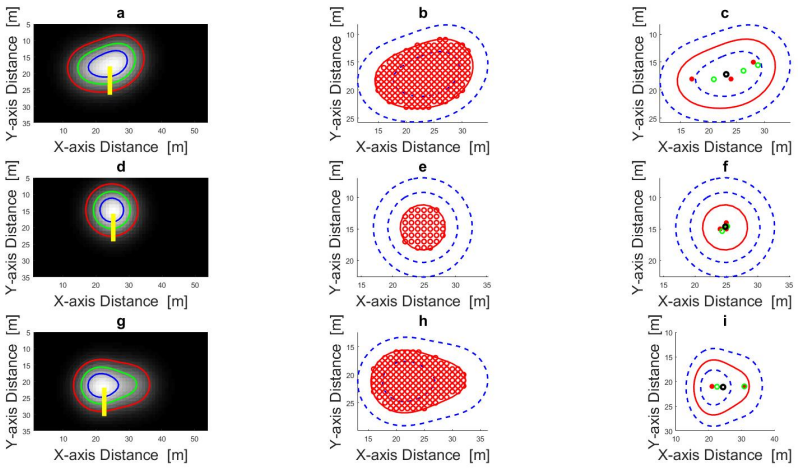

Figure 5: **Source Localization:** A radiation field is classified into a finite number of contour lines in **(a, d, g)** using log gradient classifier. Contour generation process is automatically terminated depending on similarity in shape analysis and uniform samples are taken inside the ROI contour in **(b, e, h)**. In **(c, f, i)** red dots are the actual sources, black circles are the estimated sources by Hough transform and green circles are the estimated sources by proposed algorithm.

the HT. NDS1, NDS2, NDS3 are the Euclidean distance between the nearest estimated source and the actual sources, respectively. In Fig. 5 (c), (f), (i), the red dots is the actual sources while the black circles and the green circles are the estimated sources using the HT and the VB algorithm, respectively.

The performance achieved by VB is outstanding and very close to the original source location. It takes at most 264 iterations to converge to the resulting state. This improvement is achieved with a gathering of real measurement data inside the ROI contour. There are several reasons that the estimated sources do not exactly converge to the true state. This could happen because of the linearization error and the inverse problem [2]. Despite the variation in the true source positions, the worst case estimated error for the VB is $4.490m$ while the maximum estimated error for the HT is $10.837m$.

6.3. The Effect of ROI selection in localization

The selection of ROI contour is particularly important because the superfluous sources are eliminated as the method converges to a solution, thereby leading to an accurate localization of the sources. To visualize the effect of ROI

Table 1: Sources estimation

Src. type	**Method**	**No. Src. (ground truth)**	**NDS1**	**NDS2**	**NDS3**
Scatter	VB	3 (3)	4.490	2.618	1.942
	HT	1 (3)	4.490	2.618	7.758
Cluster	VB	2 (3)	0.778	1.399	1.604
	HT	1 (3)	0.778	1.408	1.707
Biased	VB	2 (3)	2.570	0.998	2.502
	HT	1 (3)	10.837	0.998	10.687

selection, we have repeated previous experiments, and for each of them, sequentially selected all the contour lines, and estimated the source positions using the VB. In this setup, four contour lines are assigned by the proposed classifier. The index of the contour line is counted from the outer periphery. The effect of ROI can be seen in Fig. 4, which presents several results with the selection of the different ROI contours. From the analysis of Fig. 5, one can easily infer that the contour indexed 4, 2 and 3 are the ROI contours if we use the proposed strategy. In order to analyze the effect of the ROI selection, we compute the estimation error similar to the algorithm 4 for each contour index and plot them in Fig. 7. The estimation errors are also shown for the clustered, biased and scattered sources. Comparing to the ground truth denoted in the same Fig. 6, it is obvious from Fig. 7 that most estimation errors converge to a minimum level with the proposed ROI selection. Even though the proposed algorithm failed to show a minimum estimation error for the scattered sources as in Fig. 6, we can see that all the sources are bounded by the ROI contour line and the selected ROI contour is very close to the smallest loop, numerically, less than $2m$ away from the actual sources. This performance is achieved by a tight lower bound on the ROI area. The measurement likelihood is then generated with high-density sampling in the ROI area, as it is well known that the performance of VB excels with the increment of sampling density [25]. However, if ROI contour is failed

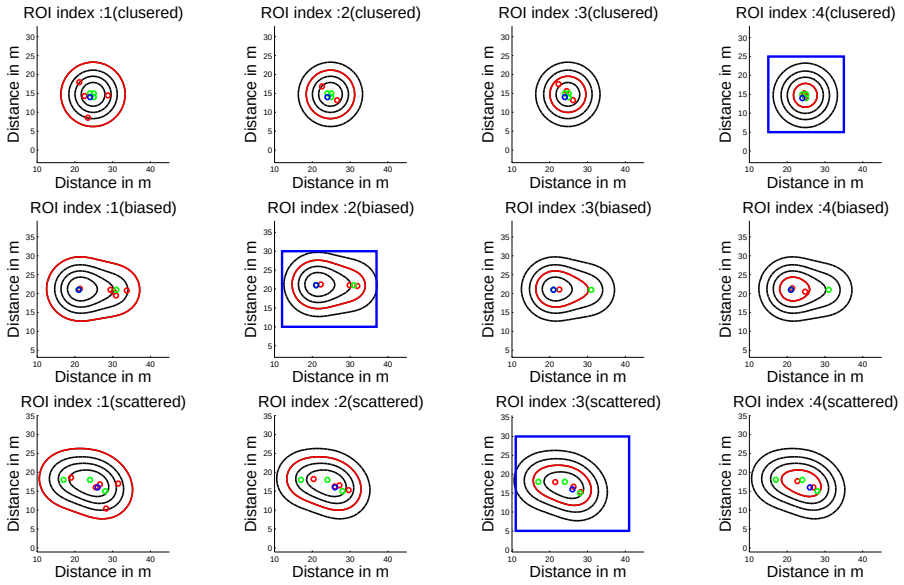

Figure 6: **The effect of ROI selection :** In this simulation, we compare the estimation accuracy w.r.t. the ROI selection. The ROI contour selected by the proposed strategy is denoted in the subfigure using the blue rectangular box. The source estimation simulations are carried out by the selection of a contour line starting off the outer periphery of the distribution. The red, blue and green circles are the estimated sources by the VB, estimated sources by the HT and the ground truth positions. It is observed that the ROI selection not only reduce the exploration space but also enhance the estimation accuracy.

to enclose all the sources, the performance of VB deteriorates due to inadequate samples.

On the other hand, the estimation of the HT depends on the geometric shape of the contour lines. Fig. 8 shows how the estimation of the HT could be changed depending on the geometric shape. However, in the case of round shapes, the HT has always found the same center of the distribution even though the ROI contour is different. Thus, the ROI selection does not have a significant impact on the source localization, but only to prohibit the UAV from performing additional contour discovering processes.

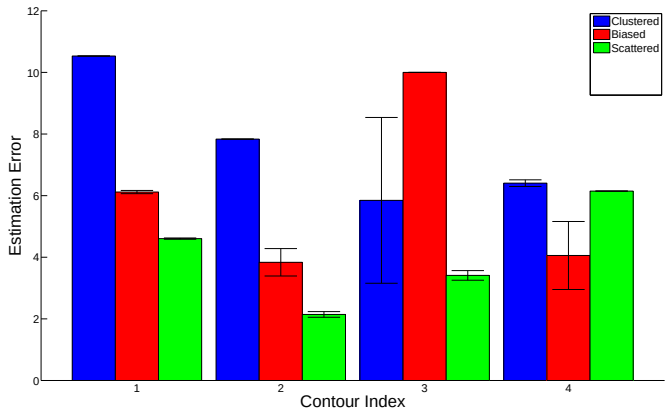

Figure 7: **Estimation error:** The estimated errors are using Algorithm 4. The results are computed with the mean over 100 simulations where the error bar represents the variation. The blue, red and green bars represent the estimation error for the clustered, biased and scattered sources. The minimum errors for the clustered, biased and scattered sources are found for the contour indices 4, 2, 3 respectively while the selected ROI contour indices using the proposed strategies are 4, 2, 2 respectively. Even though the proposed strategies does not find the optimal solution for the scattered sources, the estimation error is very close to the minimum error and bounded by the $2m$ distance.

6.4. Performance of the adaptive framework

Comparing the localization accuracy and considering the exploration constraints, the proposed adaptive method is a very efficient yet accurate solution. In general, we have found that there is a way out to optimize the localization process if the ROI contour can be accurately selected and analyzed. For comparing the performance of the adaptive method, we applied a slightly different metric: we looked at the estimation error and the length of traveled path which is required to perform each of the algorithms. Fig 9 shows the error convergence properties of each method. Since the estimated sources are different w.r.t. the ground truth sources, we then compute the average estimation error w.r.t. the nearest estimated sources similar to Algorithm 4. The simulations were performed into two phases. In the first phase, all the simulations were conducted independently without considering the ROI selection method. In order to com-

Table 2: Exploration efficiency

Parameters	**Clustered**		**Biased**		**Scattered**	
	Path Len. (m)	Estimation Error (m)	Path Len. (m)	Estimation Error (m)	Path Len. (m)	Estimation Error (m)
a path without ROI + VB	226.92	5.5	330.85	3.11	352.55	3.25
a path without ROI +HT	53.44	5.95	66.78	3.25	68.41	7.02
a path with ROI + HT	19.77	1.15	51.16	2.25	41.01	2.05
a path with ROI + VB	30.84	0.95	189.00	1.25	122.18	1.75

pute the estimation error, we combine 100 simulation results and plot the mean estimation error with variance. Even though the ROI selection does not have any influence to estimate the sources in the first case, it is obvious from the Fig. 9 that the VB outperforms the HT except for the clustered sources.

Table 2 demonstrates the efficiency of the proposed framework. It is interesting to note that the sensitivity of the source localization manifest in the ROI selection criteria. Looking at Table 2, one can see that the estimation error calculated at the VB along with the ROI and the HT along with ROI are very close only for the clustered sources, numerically $0.95m$ and $1.15m$. In that situation, a rapid solution without any additional exploration in the ROI can then be generated using the HT, results in $19.77m$ path to travel instead of $30.84m$ path.

However, the significance of the ROI selection can be verified by the Fig. 9 (b). While the maximum and minimum mean estimation error without the ROI selection method were around $7m$ and $3m$ respectively, in the second case (with the proposed ROI selection method), the maximum and minimum errors converged to $2.25m$ and $0.85m$ respectively. It is observed from the table 2 that regardless of the specific ROI, the VB always outperformed the HT. However, in the first case, the estimation error of the VB is more sensitive for the biased sources. As observed in Fig. 7, the wrong ROI selection caused a large estimation error. Thus, the better results can be achieved only with the appropriate ROI selection. It is also obvious from the table 2 that the number of samples points without a ROI selection method cannot improve the estimation accuracy.

As a result, the path required for the VB algorithm is usually longer without the ROI selection than the path with the ROI selection. Despite the more sampling points by the longer path, the estimation accuracy is always better in the case of a path with the ROI selection, shown in the table 2.

Algorithm 4 Compute estimation error

Require: $source, estimation$

Ensure: $averageError$

$mse \leftarrow \{\}$
$averageError \leftarrow 0$
for $i = 0$ **to** $size(source)$ **do**
  for $j = 0$ **to** $size(estimation)$ **do**
    $x_s \leftarrow source(i, 1)$
    $x_e \leftarrow estimation(j, 1)$
    $y_s \leftarrow source(i, 2)$
    $y_e \leftarrow estimation(j, 2)$
    $mse \leftarrow mse \cup sqrt((x_s - x_e)^2 + (y_s - y_e)^2)$
  end for
  $averageError \leftarrow averageError + min(mse)$;
end for
$averageError \leftarrow averageError/size(source)$;

Since HT generates optimal results for clustered sources, we can then extend its applications to a collection of isolated sources. However, the localization of isolated sources is beyond the scope of this paper. For a collection of a point sources, if one begins with the VB method which is explained in this paper, then the VB can converge to a solution but with poor estimation. The reason why the performance of VB is poor is that our proposed method is designed focusing on the single hotspot with multiple sources. In the case of isolated sources, there is multiple hotspot exist in the same radiation field. These results support two conclusions. First, the estimation of the VB always provides the better solution than the HT with the expense of additional exploration. Second, HT

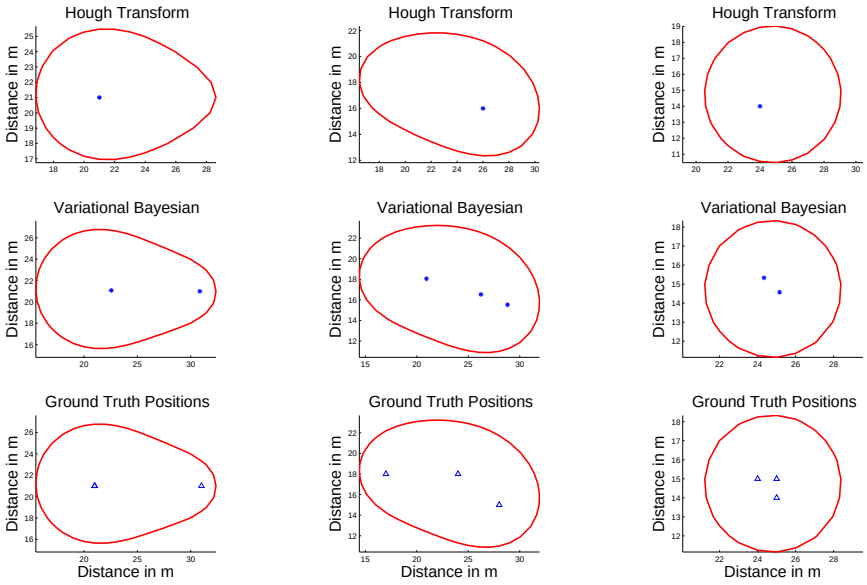

Figure 8: **Performance analysis :** Source localization simulations are carried out by the HT and the VB independently. The simulations are conducted in three types of spatially distributed sources, namely, biased, scattered and clustered. It is observed that the localization accuracy of HT is better only for the clustered sources. In the case of biased and scattered sources, the VB leads the solution to the close proximity of the ground truth positions. The ground truths are shown in the last row with the triangular shape.

can drastically reduce the exploration expense, but the desired results can be obtained only for the clustered sources.

7. Conclusion

A single UAV exploration based multiple unknown radiation sources localization problem is investigated in this study. Three different cases of spatial distributed sources are considered to demonstrate the efficiency of the proposed algorithms. In order to explore a large radiation field using a UAV, we propose to adopt a topographic mapping strategy along with the reduction of ROI in the field. The segmentation of a large radiation field was primarily done by a

novel log-gradient classifier (lgc) that segregates a priori known trajectory coupled with measurements. The trajectory connects the lower intensity region to the hotspot region of the field, where the lgc segmentes it into a finite number of interested positions. The contour lines are then generated by tracking a constant intensity value. However, the similarity analysis of contour shape indicates that the ROI in an unknown radiation field can be further reduced by avoiding superfluous contour lines.

In order to localize the radiation sources, the mitigation strategy such as proposed framework is demonstrated to be effective optimizing the trade-off between the cost of robotic exploration and the accuracy of source localization. Reducing the ROI could potentially be effective in making the robot aware of sources positions. The diagnostic criterion used for analyzing the ROI shape can be extended to predict the type of distributed sources. Although the radiation sources might be arbitrary located in an unknown radiation field, the proposed framework not only accelerates the mission completion time but also leads to accurate estimation close to actual sources. In the numerical simulation, it can be seen that with the proposed ROI selection method the VB clearly outperforms the HT in terms of accuracy. To determine the clustered sources, the HT can easily show a as similar performance as the VB without any additional exploration. Thus, the proposed framework opted the HT only for the clustered cases, otherwise, the VB is adopted.

Since we have shown that it is possible to quickly localize the sources by a single UAV, our future work will be devoted to extend the proposed framework for rapidly cover a very large areas using multiple UAVs. Furthermore, carrying out real world experiments is also of the research interest.

References

[1] J. Towler, B. Krawiec, K. Kochersberger, Radiation mapping in post-disaster environments using an autonomous helicopter, Remote Sensing, 1995-2015.

[2] M. R. Morelande, A. Skvortsov, Radiation field estimation using a gaussian mixture, in: Information Fusion, Int'l Conf. on, 2247-2254, 2009.

[3] B. Charrow, V. Kumar, N. Michael, Approximate representations for multi-robot control policies that maximize mutual information, in: Robotics: Science and Systems, 2013.

[4] C. Wang, C.-Y. Lin, M. Tomizuka, Statistical learning algorithms to compensate slow visual feedback for industrial robots, ASME Journal of Dynamic Systems, Measurement, and Control.

[5] P. Dames, M. Schwager, V. Kumar, D. Rus, A decentralized control policy for adaptive information gathering in hazardous environments, in: Decision and Control, IEEE Conf. on, 2807-2813, 2012.

[6] R. Cortez, X. Papageorgiou, H. Tanner, A. Klimenko, K. Borozdin, R. Lumia, W. Priedhorsky, Smart radiation sensor management, IEEE Robotics & Automation Magazine, 15(3):85-93.

[7] G. F. Knoll, Radiation detection and measurement, John Wiley & Sons, 2010.

[8] S. Bashyal, G. K. Venayagamoorthy, Human swarm interaction for radiation source search and localization, in: Swarm Intelligence Symposium, IEEE, 1-8, 2008.

[9] M. Reggente, A. J. Lilienthal, Using local wind information for gas distribution mapping in outdoor environments with a mobile robot, in: Sensors, IEEE, 1715-1720, 2009.

[10] N. Cao, K. H. Low, J. M. Dolan, Multi-robot informative path planning for active sensing of environmental phenomena: A tale of two algorithms, in: Int'l Conf. on Autonomous agents and multi-agent systems, 7-14, 2013.

[11] R. Cortez, H. Tanner, Radiation mapping using multiple robots, in: Emergency Preparedness and Response and Robotic and Remote Systems, ANS Int'l Joint Topical Meeting on, 157-159, 2008.

[12] J. Han, Y. Chen, Multiple uav formations for cooperative source seeking and contour mapping of a radiative signal field, Jour. Intelligent & Robotic Systems, 323-332.

[13] G. Hitz, A. Gotovos, F. Pomerleau, M.-E. Garneau, C. Pradalier, A. Krause, R. Y. Siegwart, Fully autonomous focused exploration for robotic environmental monitoring, in: Robotics and Automation, IEEE Int'l Conf. on, 2658-2664, 2014.

[14] K. H. Low, J. M. Dolan, P. Khosla, Adaptive multi-robot wide-area exploration and mapping, in: Int'l Conf. on Autonomous agents and multiagent systems, 23-30, 2008.

[15] Y.-H. Kim, D. Shell, Distributed robotic sampling of non-homogeneous spatio-temporal fields via recursive geometric sub-division, in: Robotics and Automation, IEEE Int'l Conf. on, 557-562, 2014.

[16] N. Ghods, M. Krstic, Source seeking with very slow or drifting sensors, Journal of Dynamic Systems, Measurement, and Control, 044504-044508.

[17] S.-i. Azuma, M. S. Sakar, G. J. Pappas, Stochastic source seeking by mobile robots, Automatic Control, IEEE Transactions on, 2308-2321.

[18] M. S. Stanković, D. M. Stipanović, Extremum seeking under stochastic noise and applications to mobile sensors, Automatica, 1243-1251.

[19] A. Ghoshal, D. Shell, Covering space with simple robots: from chains to random trees, in: Robotics and Automation, IEEE Int'l Conf. on, 914-920, 2013.

[20] A. Gunatilaka, B. Ristic, R. Gailis, On localisation of a radiological point source, in: Information, Decision and Control, 236-241, 2007.

[21] A. Krause, C. Guestrin, Near-optimal observation selection using submodular functions, in: AAAI Conf. Artificial Intelligence, 1650-1654, 2007.

[22] K. H. Low, J. M. Dolan, P. K. Khosla, Information-theoretic approach to efficient adaptive path planning for mobile robotic environmental sensing., in: Intl Conf. Automated Planning and Scheduling, 2009.

[23] D. G. Tzikas, A. C. Likas, N. P. Galatsanos, The variational approximation for bayesian inference, Signal Processing Magazine, IEEE, 131-146.

[24] M. Chen, Variational bayesian inference for gaussian mixture model (2012).
URL http://www.mathworks.com/matlabcentral/fileexchange/35362-variational-bayesian-inference-for-gaussian-mixture-model

[25] B. Wang, D. Titterington, Convergence properties of a general algorithm for calculating variational bayesian estimates for a normal mixture model, Bayesian Analysis, 625-650.

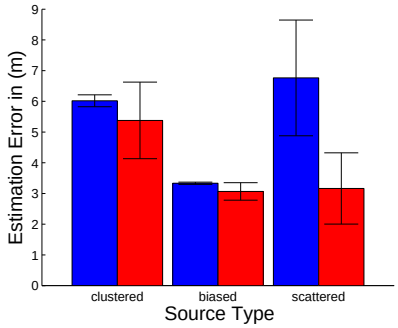

(a) without the ROI selection

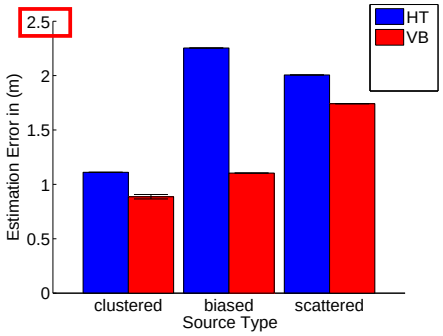

(b) with the proposed ROI selection

Figure 9: **The analysis of error convergence :** The performance of the HT and VB is evaluated w.r.t the nearest estimated source location. The estimation error is computed over 100 iterations using algorithm 1 with (a) all possible combination of the ROI selection (b) with the proposed ROI selection. The red bar is the estimation error of the VB and the blue bar is of the HT. It is obvious that the VB outperforms the HT in terms of estimation accuracy. It note worthy that the outstanding error convergence can be obtained only with the proposed ROI selection method.